Bulletin of the Seismological Society of America, Vol. 107, No. 5, pp. 2067–2077, October 2017, doi: 10.1785/0120160123

A Regional Site-Response Model for the Groningen Gas Field

by Adrian Rodriguez-Marek, Pauline P. Kruiver, Piet Meijers, Julian J. Bommer, Bernard Dost, Jan van Elk, and Dirk Doornhof

Abstract A key element in the assessment of seismic hazard and risk due to induced earthquakes in the Groningen gas field is a model for the prediction of ground motions. Rather than using ground-motion prediction equations with generic site amplification factors conditioned on proxy parameters such as V_{S30}, a field-wide zonation of frequency-dependent nonlinear amplification factors has been developed. Each amplification factor is associated with a measure of site-to-site variability that captures the variation of V_S profiles and hence amplification factors across each zone, as well as the influence of the uncertainty in the modulus reduction and damping functions for each soil layer. This model can be used in conjunction with the predictions of response spectral accelerations at a reference rock horizon at a depth of about 800 m to calculate fully probabilistic estimates of the hazard in terms of ground shaking at the surface for a large region potentially affected by induced earthquakes.

Introduction

Gas production in the Groningen field in the northern Netherlands began more than 50 years ago and the reserves—the seventh largest in the world—are now 70% depleted, which has led to compaction of the reservoir and consequently the re-activation of geological faults. The first perceptible earthquake in the field occurred some 15 years ago and these induced events have become more frequent in recent years. In response to these earthquakes, the field operator Nederlandse Aardolie Maatschappij B.V. is undertaking probabilistic assessments of the consequent seismic hazard and risk both as a requirement of the production license application and also to inform decision-making regarding building, strengthening, and other risk mitigation measures.

A key element of the induced seismic hazard and risk models is a ground-motion prediction model. The risk analysis is performed for the entire field plus a buffer zone of 5 km (for onshore areas), which covers a region some 50 km × 40 km in extension. There is inevitably large uncertainty in the prediction of ground motions from potential earthquakes of larger magnitude. Expanding networks of accelerographs have yielded a useful database of surface recordings but these are limited to events no greater than the largest earthquake that occurred (in August 2012), which had a local magnitude M_L of 3.6. An element of the ground-motion prediction model for which reduction in epistemic uncertainty was feasible even without the occurrence of larger earthquakes was the influence of the local site-response characteristics. The near-surface deposits are expected to exert an appreciable influence on the ground motions, because nearly the entire area is overlain by thick layers of deltaic deposits with an average 30-m shear-wave velocity V_{S30} of about 200 m/s. Therefore, rather than using generic site amplification factors (AFs) conditioned on a surrogate parameter like V_{S30}, a major effort was made to develop region-specific amplification functions that also capture the nonlinear response of these soft soils under higher levels of shaking. This article describes the development of this regional site amplification model for Groningen, starting with a brief overview of how the model is constructed and how it is deployed in the hazard and risk calculations. The subsequent sections describe each element of the model development in greater detail. The article concludes with a brief discussion of potential refinements and improvements to the model that may be addressed in future work.

Overview of the Site-Response Model

To include local site effects on surface ground motions in the Groningen field, the current ground-motion prediction model combines ground-motion prediction equations (GMPEs) for response spectral accelerations at a reference rock horizon with nonlinear site AFs assigned to zones covering the entire study area. The seismic hazard and risk calculations are performed using Monte Carlo simulations (Bourne *et al.*, 2015), which allow a fully probabilistic incorporation of site response into ground-motion predictions. For each ground-motion realization at the rock horizon, the site AF is applied contingent on the actual rock motion—including the randomly sampled components of variability—rather than the median motions for the magnitude–distance scenario. The site AF is also applied randomly, sampling from the site-to-site variability. Although computationally more intensive than the convolution approach proposed by Bazzurro and Cornell (2004), the framework adopted for

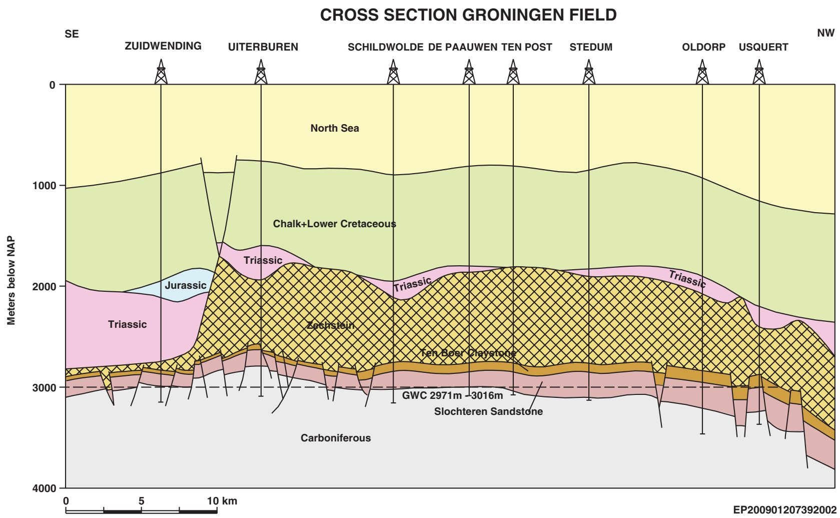

Figure 1. Geological cross section through the Groningen gas field (source: Nederlandse Aardolie Maatschappij B.V. [NAM]). NAP, Dutch Ordnance Datum.

Groningen is effectively Approach 4 rather than Approach 3 based on that proposal (McGuire *et al.*, 2001).

Once the reference rock horizon was selected, the first stage of building the model was to construct a layered model of the shear-wave velocities V_S down to a specified elevation across the entire field; this stage of the work is described in detail in Kruiver *et al.* (2017). An estimate of the uncertainty in the V_S profiles was required, together with a scheme for randomization of the profiles in the site-response analyses. Mass densities were assigned to each layer and then modulus reduction and damping (MRD) functions were selected for each of the layers. The site-response analyses were performed using 1D models for vertically propagating shear waves, as is common practice. For practical reasons, we also decided to perform the site-response analyses in the frequency domain using random vibration theory (RVT) as coded in the program Strata (Rathje and Ozbey, 2006; Kottke and Rathje, 2008). This approach is much more efficient (in terms of preparation of the inputs) than using time-history analyses, and tends to yield slightly higher results (Kottke and Rathje, 2013); the small conservative bias was considered a reasonable penalty for the gains in efficiency given that site-response analyses were conducted at more than 140,000 locations. The choice of RVT-based site-response analyses rather than a time-domain approach automatically restricted the analyses to equivalent linear (EQL) rather than fully nonlinear methods. Although it is known that EQL analyses may introduce errors at large strains (Kaklamanos *et al.* 2013), the need for an efficient platform conditioned the choice of this method. Given how soft the local soil deposits are, the consequences of this decision are important and are discussed in terms of modeling uncertainty.

The calculated site AFs are grouped into zones—for the most part, these coincide with the geological zonation presented by Kruiver *et al.* (2017)—for which a single AF is then defined for each of 23 oscillator periods between 0.01 and 5 s. Each nonlinear AF is accompanied by a site-to-site variability that reflects the variation of the profiles across the zone, the inherent variability in the site AF due to variability in the profiles, the dynamic soil properties and the input motions, and additional factors related to modeling uncertainty. This field-wide zonation map is then implemented into the probabilistic seismic hazard and risk calculations (Bommer *et al.*, 2017).

Site Characterization Model

To develop the site amplification functions for the Groningen field, the first stage of the work was to create layer models for individual locations within the entire area, using the defined reference rock horizon to the ground surface.

Reference Rock Horizon

Figure 1 shows a geological cross section through the Groningen field. The gas reservoir exists within the Slochteren sandstone at a depth of about 3 km; it is overlain by the Zechstein salt layer and then a 1 km layer of chalk. A pronounced impedance contrast, which is at an average depth of ~800 m, exists at the base of the North Sea Supergroup. This horizon is chosen as the reference rock horizon that is treated as the top of an elastic half-space in the site-response calculations. The shear-wave velocity at this horizon is very close to 1400 m/s (Kruiver *et al.*, 2017).

The reason for selecting the reference rock at this horizon is simply that this is the first elevation at which a strong and persistent velocity contrast is encountered. Another velocity contrast is encountered at a depth of about 400 m at the Brussels Sands formation, but at 100 m below this elevation a velocity reversal makes it unsuitable as the top of an elastic half-space. Moreover, the Brussels Sands formation is not consistently mapped across the entire field.

The base of the North Sea Supergroup (hereafter, NS_B) is well defined over the entire study region. Because of the shallow focus of the earthquakes, which are located within the gas reservoir, this choice has the rather unusual consequence that for the sites close to the epicenter, approximately one-quarter of the travel path is modeled by the site amplification functions.

Layer Models: Shear-Wave Velocity and Density

The velocity model from the NS_B horizon to the ground surface is described in detail by Kruiver *et al.* (2017), and only a brief summary is presented herein. The velocity model from the surface to 50 m below the Dutch Ordnance Datum is built from a geostatistical model, the GeoTOP model, with a 100 × 100 m spatial resolution that assigns a stratigraphic unit and a lithological class to 0.5-m thick voxels (Stafleu *et al.*, 2011). The GeoTOP V_S model also

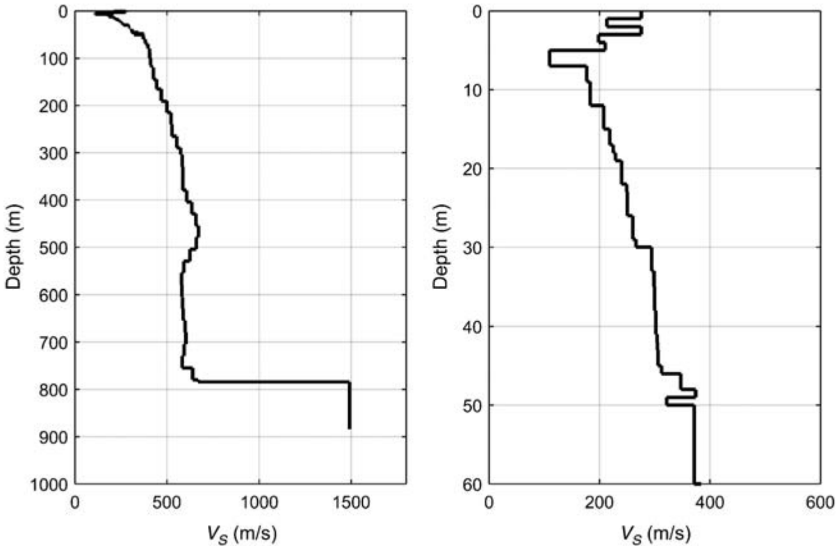

Figure 2. Sample V_S profile at the location of ground-motion recording station G09 (Bommer *et al.*, 2017). The plot on the left is the full profile down to the elastic half-space. The plot on the right is an enlarged view of the top 60 m.

includes a look-up table, which correlates each stratigraphic lithological unit to soil parameters (mean and standard deviation). These parameters include shear-wave velocity, soil density, coefficients of uniformity, median grain-size diameter, cone penetration test (CPT) tip resistance, and undrained shear strength. When observed, depth dependency of shear-wave velocity is included in these correlations. For depths greater than 50 m, velocities are assigned from the analysis of surface waves collected in field-wide experiments at the Groningen sites. These measurements extend the V_S profile to a depth of about 120 m and are described in more detail in Kruiver *et al.* (2017). Below this depth, measurements from sonic logs in the field are used to extend the profiles to the reference rock horizon (Kruiver *et al.*, 2017). The uncertainty in shear-wave velocities for depths greater than about 50 m was ignored, because these uncertainties have little impact on computed AFs. An example of the resulting V_S profiles is shown in Figure 2.

Profiles of soil unit weight are also needed for the site-response analyses. The assignment of unit weight is based on representative values for stratigraphic lithological units derived from CPTs using Lunne *et al.* (1997). For some of the deeper formations, the density is assumed to be constant, consistent with the borehole logs from two deep boreholes (Kruiver *et al.*, 2017).

Modulus Reduction and Damping Curves

The soil layers included in the site-response models comprise various sands, clays, and peats. For each of these layers, MRD functions are required to model the nonlinear behavior of the soils under higher levels of acceleration that lead to greater shear strains. Such MRD curves are typically obtained from laboratory tests, such as those of Darendeli (2001) and Menq (2003), which were adopted for clays and sands, respectively. The MRD curves of Darendeli (2001) are defined as a function of plasticity index and effective confining stress, the latter being computed from the unit weights estimated from the look-up table and from an assumed depth of the phreatic level of 1 m. The parameters of the Menq (2003) model are effective confining stress, the coefficient of uniformity, and median grain-size diameter. The latter two are obtained from values measured for stratigraphic lithological units in the field. Both the Darendeli (2001) and Menq (2003) curves are measured only to strains up to about 1%; hence, additional uncertainty is expected if these curves are extrapolated to predict site response for higher strain values.

The pervasive presence of peats in the Groningen field poses a particular challenge for modeling site response, especially because, as expected, these soils exert a strong influence on the dynamic response due to their low stiffness. Few empirical MRD curves derived for peats are available and the only published model (Kishida *et al.*, 2009a) is specific to peats in the Sacramento Delta in California. Studies have shown that these peats have lower dependency on confining stress than other peats (Kramer, 2000). Consequently, a considerable effort was made to obtain representative MRD curves for peats. Tests of Groningen peats are to be performed in the near future, but in their absence MRD curves were developed based on published data for peats from around the world (Seed and Idriss, 1970; Kramer, 2000; Wehling *et al.*, 2003; Kallioglou *et al.*, 2009; Kishida *et al.*, 2009a,b). Using these data, a formulation similar to the Darendeli (2001) and Menq (2003) models was adopted to derive the new curves. The model parameters were found to be primarily a function of confining stress. Figure 3 shows a comparison of the new model with that of Kishida *et al.* (2009b). The model proposed for this study has a stronger dependence on confining stress.

Recent work has shown that laboratory-based MRD curves tend to underestimate the low-strain damping inferred from recordings in downhole arrays (Elgamal *et al.*, 2001; Tsai and Hashash, 2009; Afshari and Stewart, 2015). Afshari and Stewart (2015), in an analysis of 10 downhole arrays in California, observe that small-strain damping matched to estimated Q-values work best for predicting site response at the arrays. To correct the low-strain damping values assigned to Groningen soils, we used estimates by De Crook and Wassing (1996, 2001) of the quality factor Q, measured at two borehole arrays at the east and south edges of the area under study. These measurements were made for depths below 75 m at the FSW station using the spectral ratio technique of Hauksson *et al.* (1987), and at shallower depths at the

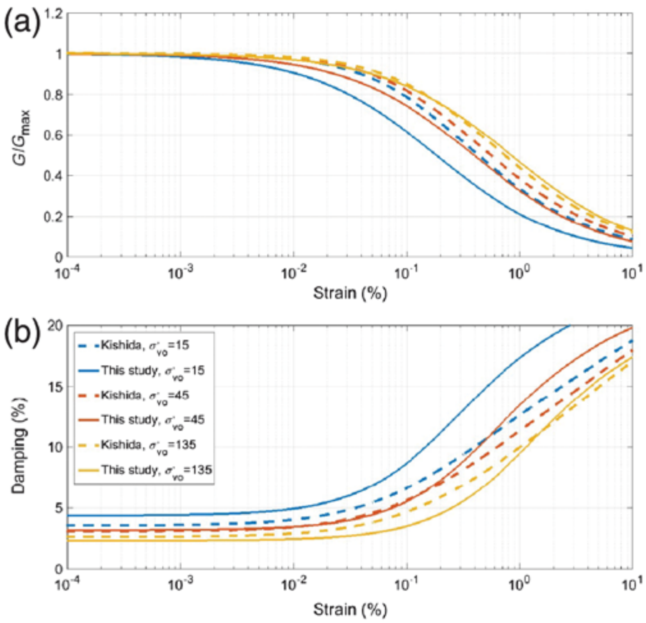

Figure 3. Comparison of modulus reduction and damping (MRD) curves obtained from the proposed model and the model by Kishida *et al.* (2009b) for different vertical effective stresses σ'_{v0}. Curves for Kishida *et al.* are shown for an organic content of 30%.

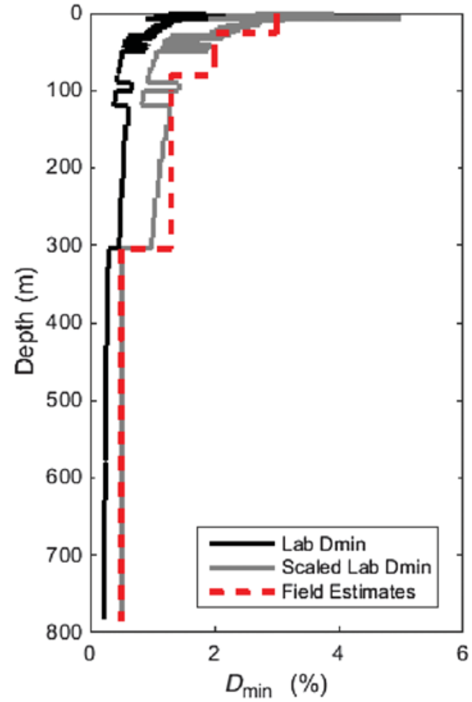

Figure 4. Low-strain damping (D_{min}) profile with depth showing laboratory estimates (Darendeli, 2001; Menq, 2003) and field estimates, along with the field-wide estimated values. The damping curves used in this study are the scaled laboratory curves. The curve shown is for the location of the G40 borehole array.

ZLV borehole array using a seismic vibrator and depth recordings at depth intervals of 1 m (De Crook and Wassing, 2001). The quality factor can be converted into the low-strain damping D_{min} using

$$D_{\mathrm{min}} = \frac{1}{2Q}. \quad (1)$$

The best estimated field-wide estimate of the low-strain damping D_{min} is shown in Figure 4. The Q-values can also be used to estimate the amount that the material damping contributes to the high-frequency attenuation parameter κ (Anderson and Hough, 1984). This contribution, termed $\Delta\kappa$, is given by Campbell (2009):

$$\Delta\kappa = \int_0^{z_{\mathrm{rock}}} \frac{1}{Q(z)V_S(z)} dz, \quad (2)$$

in which z_{rock} is the depth of the elastic half-space.

The damping values obtained from the methodology explained in the previous paragraph are consistent with Groningen site conditions and are higher than the low-strain damping (D_{min}) from laboratory-based curves of Darendeli (2001) and Menq (2003). However, the Menq and Darendeli curves have the advantage of capturing the D_{min} dependence on soil type and soil properties. Hence, we used a hybrid approach in which laboratory-based D_{min} values are modified to match the $\Delta\kappa$ measured at the borehole sites. Using the V_S profiles at the recording stations, we computed a factor to modify the low-strain damping values from Darendeli (2001) and Menq (2003) such that the equivalent $\Delta\kappa$ is equal to that measured at the downhole array (Fig. 4). An average factor of 2.11 was obtained from all the recording stations. The low-strain damping (D_{min}) of Menq and Darendeli was then multiplied by this factor, with an upper limit of 5% set for this parameter, to constrain damping to a reasonable value. In effect, this resulted in a shift of the damping curves at all strain levels (Fig. 5). This shift is consistent with the hypothesis that the difference in laboratory and field estimates of D_{min} is due to scattering effects in the field, which should be independent of strain levels. This approach also implies that the phenomena that lead to high-frequency attenuation (e.g., material damping and scattering) are captured in our 1D analyses through equivalent viscous damping. The damping for the Lower North Sea Group, which is encountered at depths greater than about 350 m, was set to 0.5%. The Lower North Sea Group mainly consists of unconsolidated sediments consisting of sands, marls, and clays. The consistency is mainly dense glauconitic sand and hard clay. In the upper part, cementation is present in the form of thin sandstone layers.

The Darendeli (2001) model implies a large stress-strain behavior that is not necessarily compatible with the shear strength of the soil. For this reason, a model to impose a limiting shear strength at large strains was implemented. We used the Yee *et al.* (2013) model with a parameter γ_l equal to 0.3%. Additionally, the undrained shear strength was increased by 30% to account for rate effects (Lefebvre and LeBoeuf, 1987; Stewart *et al.* 2014). Limiting shear

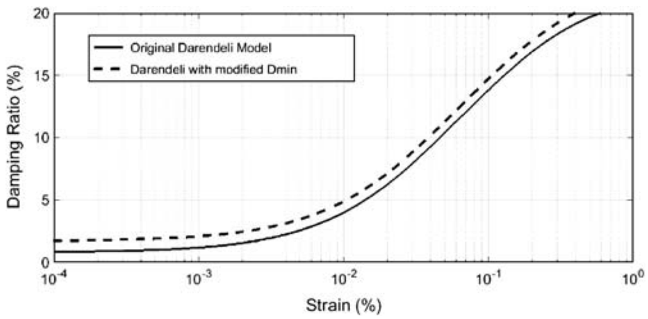

Figure 5. Original and modified damping versus strain curve for Darendeli (2001) curves illustrating the effect of modifying the low-strain damping ($D_{\min}$). The curve shown is for plasticity index = 15; overconsolidation ratio = 1; and $\sigma_0' = 1$ atm.

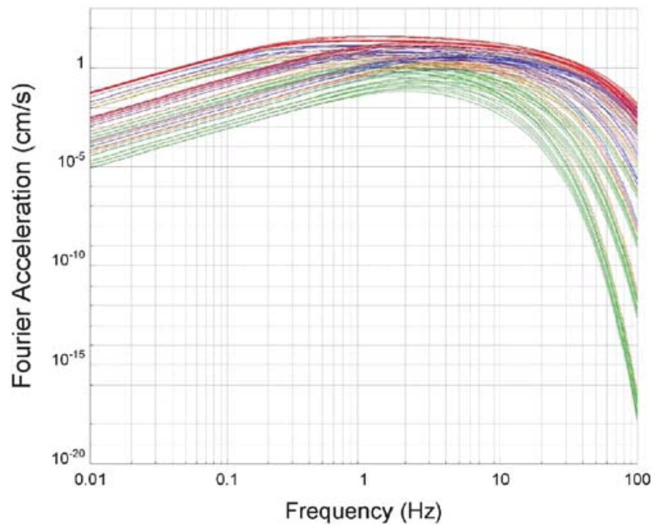

Figure 6. Fourier amplitude spectra at the base of the North Sea Supergroup (NS_B) horizon used as input to random vibration theory (RVT)-based site-response analyses. The colors indicate five groups of increasing strength of the motion.

strengths were implemented for clay, clayey sand, sandy clay, and peat. No limiting strength was used for sand layers because of their higher strengths and the lower strains typically observed in the analyses. This modification only affects the modulus reduction curve at large strains.

Input Motions and Randomizations

After defining the elastic half-space and the layer models for each location, the additional requirements to perform the site-response analyses were input motions at the reference rock horizon and a scheme for randomization of the soil properties. These two topics are briefly discussed in this section.

Reference Rock Input Motions

Because the RVT-based approach to site-response analysis was used, the inputs at the NS_B horizon are required in the form of Fourier amplitude spectra (FAS) of acceleration and ground-motion duration. Whereas the FAS would normally be obtained from response spectra defined at the top of the elastic half-space, the fact that the GMPEs for the rock motions are based on stochastic simulations (Bommer *et al.*, 2016, 2017) meant that the FAS could be generated directly. The FAS were defined using the Brune (1970, 1971) spectrum for the characteristics of the reference rock (κ_0 0.015 s) and for the three different values of stress parameters adopted to capture the range of epistemic uncertainty in the predictions. FAS were generated in this way for magnitudes 4, 5, and 6—being representative of the earthquakes driving the hazard, as inferred from disaggregations—and for each magnitude-stress drop combination at the epicenter and an additional 11 epicentral distances at regular logarithmic intervals from 1 to 60 km. The resulting 108 FAS were then classified into five groups of increasing maximum acceleration (peak ground acceleration) of the motion (Fig. 6). Five FAS were used as inputs at each of the 140,862 grid locations, each randomly sampled from the five groups to ensure an adequate range of strength to capture both the linear and nonlinear site amplification.

The durations were determined from the simulated time series of acceleration corresponding to the FAS. The duration model for the simulated time series was calibrated using Groningen recordings (Bommer *et al.*, 2017). The significant duration is defined as $D_{5\text{–}75}$, this being the interval containing 5%–75% of the total Arias intensity of the record (e.g., Bommer and Martínez-Pereira, 1999). This is consistent with the definition of duration used in the 1D-EQL-RVT site-response calculations. The $D_{5\text{–}75}$ values for the input signals range from 0.8 to 8.2 s.

Randomizations of Profile Properties

The AF for each zone must capture the spatial variability within each zone and the uncertainty of the parameters that control the site response at each location within the zone. An alternative approach would be to perform site response for randomized V_S profiles at each voxel stack and then repeat the analyses for all of the voxel stacks within a zone. This alternative implies a very large number of site-response analyses, which would actually become prohibitive given the large area for which the site amplifications were required. Another alternative, selected for this study, is to capture the spatial variability across each zone by performing site-response analyses at each voxel stack within a zone and to then capture the input parameter uncertainty by selecting a randomized profile for each voxel stack. This approach is viable because all of the zones have a large number of voxel stacks, representing the variability of stratigraphy and lithology within the zone.

Potentially, each variable that is an input to the site-response calculations can be randomized. However, for each added parameter to a randomization process, the calculation time increases exponentially. Therefore, we selected to randomize the two inputs that have the strongest effect on computed AF: shear-wave velocity in the near-surface layers (e.g., in the GeoTOP layers) and the input motions; the latter was discussed in the previous section.

The shear-wave velocity was randomized by selecting a random value of V_S at the center of each GeoTOP layer, assuming a bounded lognormal distribution with the median and standard deviations given by the look-up table. The distributions were truncated at two standard deviations; to compensate for the truncation, the V_S values were sampled from a distribution with a standard deviation that is increased by 16%.

The V_S values for each unit were assumed to be fully correlated. The unit-to-unit correlation of V_S values was assumed to be 0.5. This value is consistent with correlations observed at well-characterized sites (Rodriguez-Marek *et al.*, 2014). The correlation was implemented using a modified version of the Toro (1995) approach, which is common to most implementations of V_S randomizations.

The parameters that were not randomized were the soil density, the MRD curves, and the thickness of each soil unit. Soil density varies within limited ranges and hence its uncertainty does not have a strong effect on the AF. Layer thickness is implicitly randomized because of variations in layer thickness of voxel stacks across a zone. The uncertainty in the MRD curves, on the other hand, can have a potentially important effect on site response. The effects of MRD uncertainty on AF variability were captured in a separate exercise that is described later.

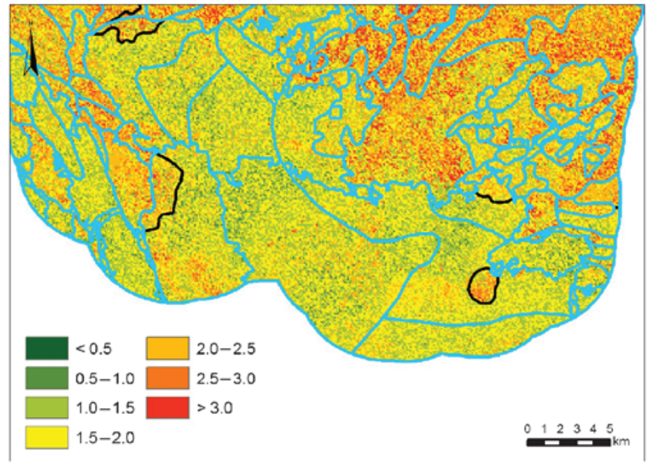

Figure 7. Linear amplification factor (AF) results for period $T = 0.1$ s from weak input motions (green signals from Fig. 6) for each of the GeoTOP voxel stacks, enlarged on the southern part of the region. Superimposed on the map are the original zonation (blue) and the adjusted zonation based on the AF results (black).

Amplification Factors and Field Zonation

The site-response analyses yielded more than 16 million frequency-dependent AFs using the randomized V_S profiles. Additionally, AFs were obtained using the mean V_S profiles, and these were used to validate the zonation map developed from the geological model (Kruiver *et al.*, 2017). Once the final zonation was defined, a model for the mean and the standard deviation of the AF for each zone was computed. The uncertainty in the AFs for each zone was then used to build a model for site-to-site variability in the AFs.

Zonation Based on Amplification Factors

The objective of the zonation of the Groningen field is to define areas of similar characteristics in terms of site response such that the AFs computed for the zone have reasonably low variability. An initial geology-based zonation map (Kruiver *et al.*, 2017) was used as a starting point for the zonation. Linear AFs were computed for each voxel stack in the field using the mean V_S profile for each voxel stack. Various zones with similar characteristics in terms of zone-averaged amplification functions were merged in a preliminary step. After this initial iteration, the AFs computed using the mean V_S profiles and low-intensity input motions were superposed on the geology-based zonation map. In general, there was very good agreement between the two (Fig. 7). The exception was a few subzones that contained AFs consistently different among various periods than their respective zones. Hence, five new zones were created to accommodate these differences (Fig. 7). This process was accomplished via a careful visual examination of plots similar to those shown in Figure 7.

Regression for Amplification Factors

The AFs computed for each voxel stack and each oscillator period were used to define amplification functions. The amplification functions were found to be strongly nonlinear, as would be expected for soft-soil profiles. The model proposed by Stewart *et al.* (2014) was used to fit the AF as a function of the input spectral acceleration (SA):

$$\ln(\mathrm{AF}) = f_1 + f_2 \ln\left(\frac{\mathrm{SA}_{\mathrm{NS_B}} + f_3}{f_3}\right) + \varepsilon\sigma_{\ln \mathrm{AF}}, \qquad (3)$$

in which f_1, f_2, and f_3 are parameters, $\mathrm{SA}_{\mathrm{NS_B}}$ is the outcropping baserock acceleration at the elastic half-space (in units of g), ε is a standard normal random variable, and $\sigma_{\ln \mathrm{AF}}$ is a parameter that represents the standard deviation of the data with respect to the median prediction of the model. Parameter f_1 represents the low-intensity (i.e., linear) response, whereas parameters f_2 and f_3 control the nonlinear response. These two parameters have a strong interaction. Hence, to obtain more stable regressions, parameter f_3 was fixed for the entire field to a period-dependent value selected during preliminary regressions. The standard deviation ($\sigma_{\ln \mathrm{AF}}$) was allowed to vary with intensity (i.e., a heteroskedastic model) following a trilinear functional form given by

$$\sigma_{\ln AF} = \begin{cases} \sigma_{\ln AF,1} & \text{for } SA_{NS_B} < SA_{rock,low} \\ \sigma_{\ln AF,1} + (\sigma_{\ln AF,2} - \sigma_{\ln AF,1}) \frac{\ln(SA_{NS_B}) - \ln(SA_{rock,low})}{\ln(SA_{rock,high}) - \ln(SA_{rock,low})} & \text{for } SA_{rock,low} \le SA_{NS_B} \le SA_{rock,high} \\ \sigma_{\ln AF,2} & \text{for } SA_{NS_B} > SA_{rock,high} \end{cases}, \tag{4}$$

in which $SA_{rock,low}$ and $SA_{rock,high}$ were set to constant field-wide values after a careful examination of preliminary regression results. The remaining parameters were determined through regression analyses, using a two-step process. First, a maximum-likelihood regression (Benjamin and Cornell, 1970) was conducted. The values of the parameter f_2 were then smoothed across periods for each zone and, for periods longer than 1 s, upper and lower bounds were set (−1.0 and 2.0, respectively). These limits represent reasonable bounds of nonlinearity for these longer periods. Finally, regression analyses were conducted again to obtain the values of parameter f_1 and the standard deviation model (equation 4).

To constrain the behavior of equation (3) when extrapolated to large input motions, limits were imposed on the values of AF. A lower limit of 0.25 was selected, such that the rock motions could not be reduced by more than a factor of 4. The upper limit on AF was defined by the data and inferred from the 98th percentile highest input motions used in the development of the AF. This upper limit only applies to longer periods (≥2 s) in which elongation of the resonant period due to nonlinearity leads to an increase of AF with increasing levels of rock motions. The parameters that are constant for the entire field are given in Table 1. The remaining parameters for all the zones are shown in Figure 8. The linear AF in each zone, shown in the top-left plot, is given as e^{f_1}. The parameter f_2 indicates the degree of nonlinear response, with a negative value indicating a decrease of AF with increasing intensity of motion. For short response periods, f_2 is always negative whereas at longer periods it sometimes assumes positive values. Figure 9 shows the resulting functions for the AF at 12 selected periods for the entire field and Figure 10 shows spatial distribution of the linear AF across the field at four selected periods. It is observed in Figure 9 that nonlinearity for an oscillator period of 0.01 s is triggered at values of SA_{NS_B} that are much lower than those typically associated with nonlinear behavior of soils. However, the input accelerations are at the reference rock horizon at a depth of about 800 m, whereas the nonlinear site response is likely to occur within the shallow (<10 m) surface layers. Therefore, the actual accelerations that trigger nonlinearity are higher than those observed in Figure 9.

Table 1
Fitting Parameters that Are Constant for the Entire Field

T (s)	f_3	$SA_{rock,low}$ (g)	$SA_{rock,high}$ (g)
0.01	0.004	0.0015	0.015
0.025	0.004	0.0013	0.0133
0.05	0.004	0.0009	0.0095
0.075	0.004	0.0018	0.0176
0.1	0.0188	0.0058	0.0577
0.125	0.0625	0.0118	0.1178
0.15	0.108	0.0177	0.1767
0.175	0.1715	0.0242	0.2419
0.2	0.256	0.0309	0.3086
0.25	0.5	0.0359	0.3589
0.3	0.5	0.0384	0.3837
0.4	0.5	0.0368	0.3679
0.5	0.5	0.0314	0.3142
0.6	0.5	0.0279	0.2786
0.7	0.5	0.0274	0.2739
0.85	0.5	0.0235	0.235
1	0.5	0.0159	0.1594
1.5	0.5	0.0092	0.0924
2	0.5	0.0053	0.0531
2.5	0.5	0.0033	0.0329
3	0.5	0.002	0.0201
4	0.5	0.0013	0.0126
5	0.5	0.0009	0.0088

SA, spectral acceleration.

Site-to-Site Variability

As discussed earlier, the standard deviations obtained from the regression analyses ($\sigma_{\ln AF}$) and expressed in equation (4) represent the joint effect of uncertainty in the soil profile model at each voxel stack and the spatial variability across voxel stacks in a zone. In addition, the $\sigma_{\ln AF}$ also include the effects of motion-to-motion variability. The development of $\sigma_{\ln AF}$ did not take into account several sources of uncertainty, including modeling error and the contribution to variability in AF due to MRD uncertainty. To construct the uncertainty model for each zone, the $\sigma_{\ln AF}$ are modified to account for these additional sources of uncertainty. The resulting uncertainty within a zone is labeled ϕ_{S2S}. The subscript $S2S$ implies that this uncertainty component represents the site-to-site variability for all sites within a given zone.

Modeling error can result from limitations of the adopted site-response procedure. In particular, various studies have shown that the EQL procedure produces biased results at large strains (Kaklamanos *et al.*, 2013, Kim *et al.*, 2016). If the modeling procedure is likely to produce a bias in the results, some adjustment should be made for this effect. One possible approach is to inflate the $\sigma_{\ln AF}$ to account for the bias. However, the EQL procedure in general results in a positive bias in computed spectral accelerations with respect to more accurate nonlinear procedures, even at large strain levels (Kottke, 2010; Kim *et al.*, 2016). Similarly, the

RVT procedure also produces positive bias with respect to time-series analyses (Kottke, 2010; Kottke and Rathje, 2013). For these reasons, it was considered that the selected RVT-based EQL analyses result in conservative biases and no modeling error was added to $\sigma_{\ln AF}$.

Empirical bounds to computed site-response uncertainty may be necessary because the 1D site-response analyses predict very limited uncertainty in site response for periods longer than the first-mode site period. On the other hand, empirical evidence shows that the site-to-site variability at long periods does not decrease significantly with increasing V_{S30}. Similar to other projects, the minimum level of epistemic uncertainty on the site term was selected based on the site-to-site variability at borehole stations in the KiK-net array

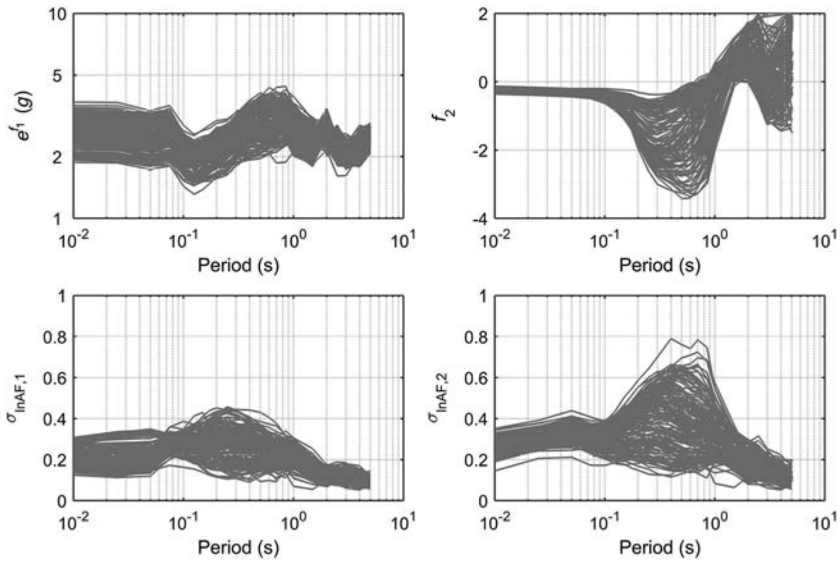

Figure 8. Parameters for all the zones in the Groningen field. The exponential of parameter f_1 is shown (top left) because it represents the small-strain (i.e., linear) amplification.

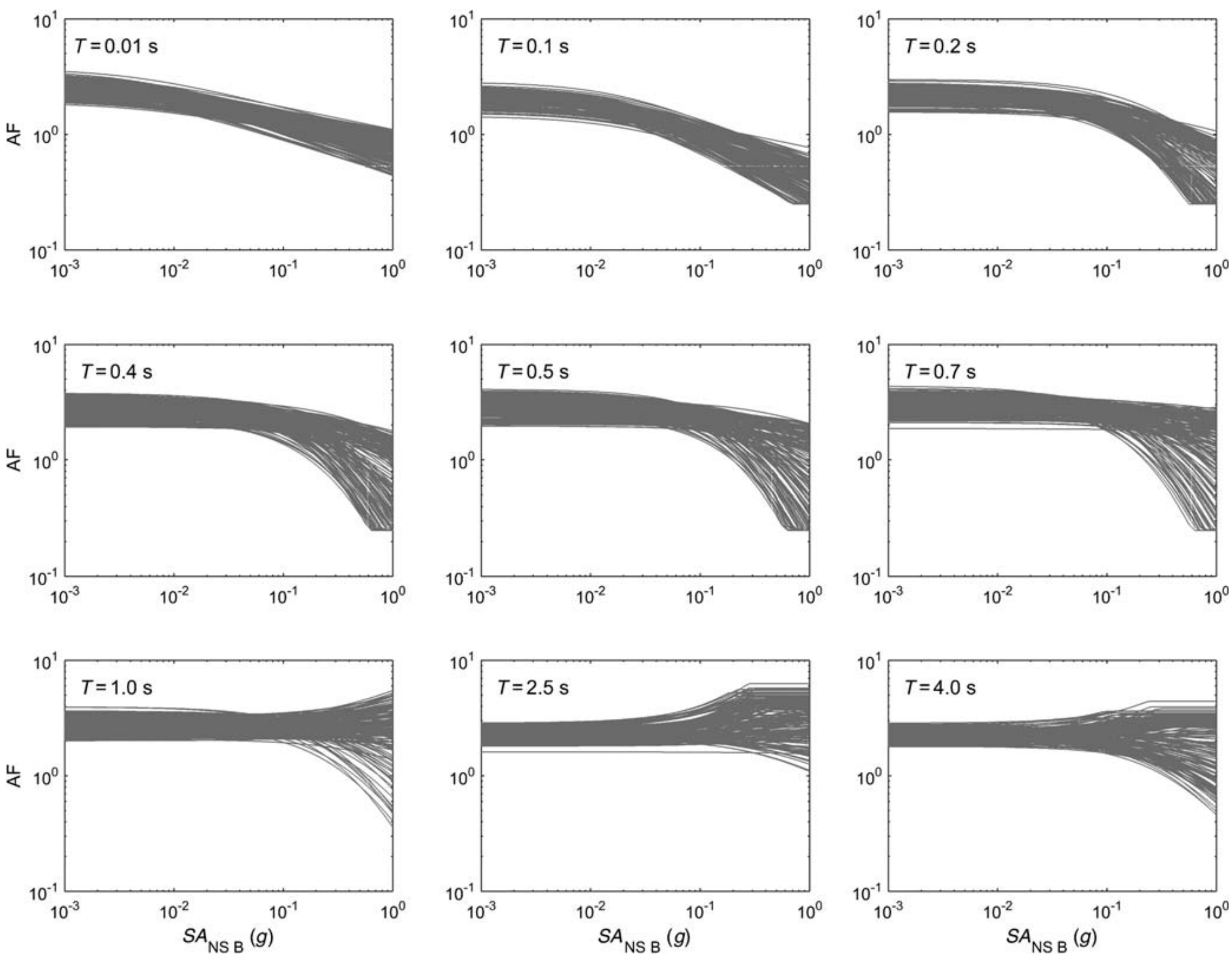

Figure 9. Fitted AF functions for all zones for selected periods.

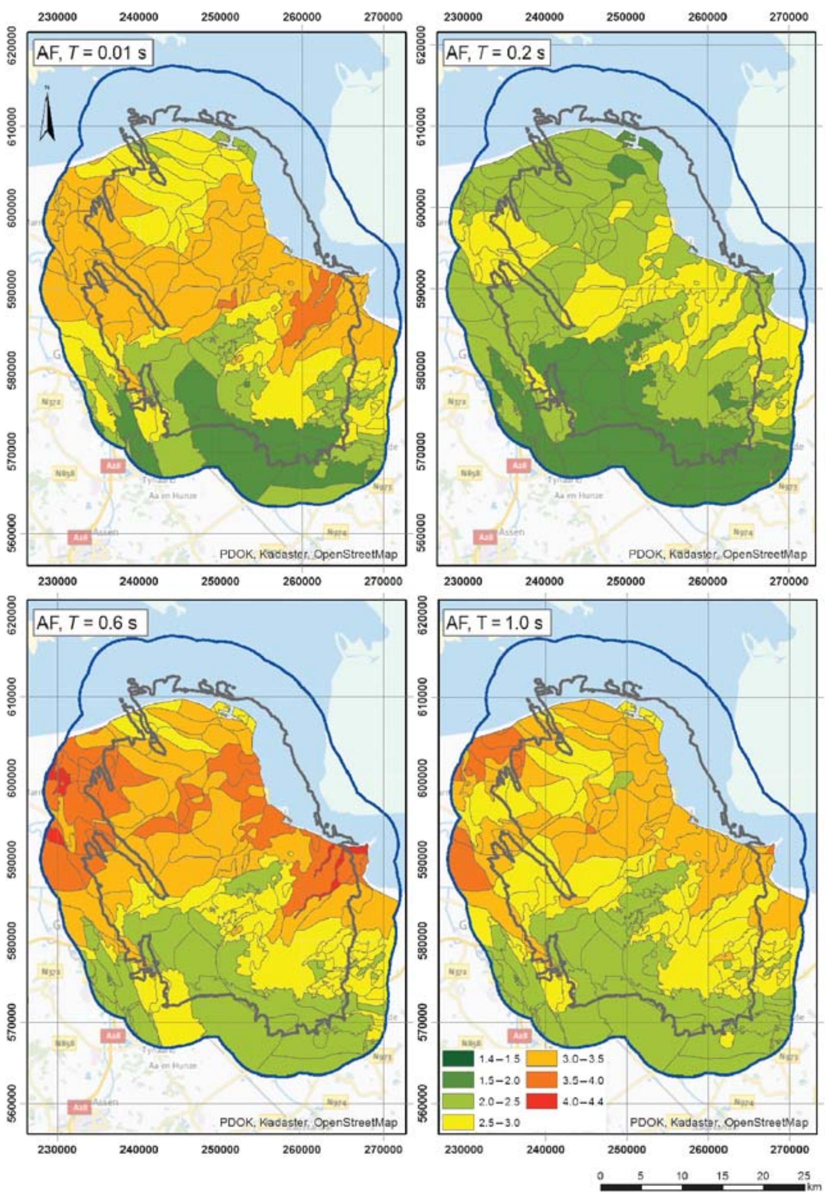

Figure 10. Fitted linear AF (e^{f_1}) for the Groningen field (selected periods).

(Rodriguez-Marek *et al.*, 2014). This variability is 0.2 in natural logarithms. The site conditions at borehole stations in the KiK-net array are relatively uniform and the site-to-site variability does not show dependence on site properties. For these stations, site response would predict almost no site-to-site variability; hence, the measured 0.2 value is considered an empirical lower bound to ϕ_{S2S}.

The additional uncertainty in the AF needed to account for the epistemic uncertainty in MRD was obtained through a modeling exercise at three selected sites within the Groningen field. This value was obtained by computing the difference in $\sigma_{\ln \mathrm{AF}}$. Computation for a full randomization was performed (i.e., V_S, input motions, and MRD curves), with the $\sigma_{\ln \mathrm{AF}}$ computed for the case in which V_S and input motions were randomized but the MRD curves were not. The randomization of MRD curves was performed using the uncertainty recommended by Darendeli (2001) and a correlation coefficient of -0.5 between damping and modulus reduction curves. The resulting contribution to $\sigma_{\ln \mathrm{AF}}$ due to MRD variability (labeled $\sigma_{\ln \mathrm{AF,MRD}}$) at the three study sites is shown in Figure 11. There are significant differences in the results for the three sites. The uncertainty also increases for higher intensity motions, reflecting the fact that for stronger motions the MRD variability combines with the motion-to-motion variability in maximum strains, leading to larger uncertainty in AF. Other studies performed similar analyses to evaluate the contribution to AF variability from V_S and MRD. Kwok *et al.* (2008) performed analyses for the Turkey Flat site and found values of $\sigma_{\ln \mathrm{AF,MRD}}$ that are lower than 0.2 for almost all periods, and lower for periods longer than the site period. Li and Assimaki (2010) performed similar analyses for the La Cienega site and also found values of $\sigma_{\ln \mathrm{AF,MRD}}$ lower than 0.2. On the other hand, Rathje *et al.* (2010) observed similar contributions to AF uncertainty from V_S and MRD, with $\sigma_{\ln \mathrm{AF,MRD}}$ values that range between approximately 0.2 and 0.3. These values were significantly larger than those computed for the three test sites at the Groningen field.

The proposed model for $\sigma_{\ln \mathrm{AF,MRD}}$ for the analyses is shown in Figure 11. The model is a conservative upper bound to the values computed at the test sites reflecting the larger values computed for other studies. The final model for the site-to-site variability in the AF is the combination of $\sigma_{\ln \mathrm{AF}}$ (equation 4) with $\sigma_{\ln \mathrm{AF,MRD}}$ in Figure 11. The model is given by

$$\phi_{S2S} = \begin{cases} \phi_{S2S,1} & \text{for } \mathrm{SA}_{\mathrm{NS_B}} < \mathrm{SA}_{\mathrm{rock,low}} \\ \phi_{S2S,1} + (\phi_{S2S,2} - \phi_{S2S,1}) \frac{\ln(\mathrm{SA}_{\mathrm{NS_B}}) - \ln(\mathrm{SA}_{\mathrm{rock,low}})}{\ln(\mathrm{SA}_{\mathrm{rock,high}}) - \ln(\mathrm{SA}_{\mathrm{rock,low}})} & \text{for } \mathrm{SA}_{\mathrm{rock,low}} \le \mathrm{SA}_{\mathrm{NS_B}} \le \mathrm{SA}_{\mathrm{rock,high}}, \\ \phi_{S2S,2} & \text{for } \mathrm{SA}_{\mathrm{NS_B}} > \mathrm{SA}_{\mathrm{rock,high}} \end{cases} \quad (5)$$

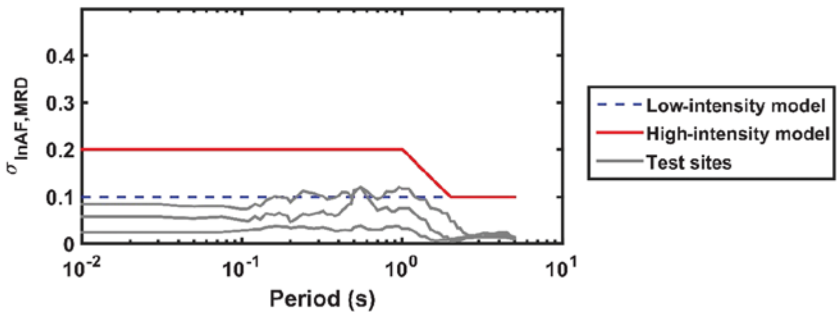

Figure 11. Contribution of MRD uncertainty to $\sigma_{\ln AF}$. The figure shows the results at three test sites and the proposed model for low- and high-intensity motions.

in which $SA_{rock,low}$ and $SA_{rock,high}$ are given in Table 1 and

$$\phi_{S2S,1} = \sqrt{(\sigma_{\ln AF,1})^2 + (\sigma_{\ln AF,MRD,\,low\ intensity})^2}$$
$$\phi_{S2S,2} = \sqrt{(\sigma_{\ln AF,2})^2 + (\sigma_{\ln AF,MRD,\,high\ intensity})^2}. \quad (6)$$

In addition, as discussed earlier, a minimum value of ϕ_{S2S} equal to 0.2 is used.

Discussion and Conclusions

We have presented a site-response model to be used in the calculation of surface ground motions due to induced seismicity, as a key input to the calculation of the resulting seismic hazard and risk. The model is exclusively applicable to the Groningen gas field in the Netherlands but the approach adopted could be applied to other locations affected by natural or induced earthquakes. Although the model is intended for a large area rather than a single site, the approach is rigorous in terms of capturing nonlinearity in the soil response and also enabling fully probabilistic estimates of the hazard in terms of ground shaking at the surface. The model for probabilistic nonlinear site amplification functions is applied in conjunction with calculations of motions at a reference rock horizon, as explained in Bommer *et al.* (2017), and takes account of the dynamic response of the full column of almost 800 m of overlying material. This approach obviates the need for proxy parameters such as V_{S30} and depth to the horizon where shear-wave velocities of 1.0 or 2.5 km/s are reached, as used in many modern GMPEs. Small-strain damping values are calibrated from measurements at only two downhole arrays. Future refinements of the model will seek to improve this estimate with additional measurements. The proposed framework enables straightforward updating and refinement of the model as additional data becomes available, whether it be from additional recordings at surface instruments and downhole arrays, *in situ* measurements of V_S, or laboratory-based calibration of modulus and damping reduction curves.

Data and Resources

The geological and velocity models are as presented in the paper by Kruiver *et al.* (2017). The near-surface geology is based on the GeoTOP model of Geological Survey of the Netherlands (TNO-GDN), whereas deeper velocity data are derived from proprietary data from Nederlandse Aardolie Maatschappij B.V. (NAM) and Shell International.

Acknowledgments

Ben Edwards provided the reference rock input motions for the site-response analyses. Pim Witlox, Bruno Zuada Coelho, and Jonathan Nuttall built the batch mode for Strata and performed the site-response calculations. Ger de Lange provided values for the parameters in the look-up table. The authors express particular gratitude to the members of an international panel of experts who provided very valuable feedback, suggestions, and criticisms at earlier stages of the model development, including at a workshop held in London in October 2015: Gail Atkinson, Hilmar Bungum, Fabrice Cotton, John Douglas, Jonathan Stewart, Ivan Wong, and Bob Youngs. The authors also thank Fabrice Cotton and an anonymous reviewer for the very constructive criticism of an earlier version of this article.

References

Anderson, J. G., and S. E. Hough (1984). A model for the shape of the Fourier amplitude spectrum of acceleration at high frequencies, *Bull. Seismol. Soc. Am.* **74,** 1969–1993.

Afshari, K., and J. P. Stewart (2015). Effectiveness of 1D ground response analyses at predicting site response at California vertical array sites, *Proc. SMIP15 Seminar on Utilization of Strong-Motion Data*, Davis, California, 22 October 2015.

Bazzurro, P., and C. A. Cornell (2004). Nonlinear soil-site effects in probabilistic seismic hazard analysis, *Bull. Seismol. Soc. Am.* **94,** 2110–2123.

Benjamin, J. R., and C. A. Cornell (1970). *Probability, Statistics, and Decision for Civil Engineers*, McGraw-Hill, New York, New York.

Bommer, J. J., and A. Martínez-Pereira (1999). The effective duration of earthquake strong motion, *J. Earthq. Eng.* **3,** no. 2, 127–172.

Bommer, J. J., B. Dost, B. Edwards, P. J. Stafford, J. van Elk, D. Doornhof, and M. Ntinalexis (2016). Developing an application-specific ground-motion model for induced seismicity, *Bull. Seismol. Soc. Am.* **106,** no. 1, 158–173.

Bommer, J. J., P. J. Stafford, B. Edwards, B. Dost, E. van Dedem, A. Rodriguez-Marek, P. P. Kruiver, J. van Elk, D. Doornhof, and M. Ntinalexis (2017). Framework for a ground-motion model for induced seismic hazard and risk analysis in the Groningen gas field, The Netherlands, *Earthq. Spectra* **33,** no. 2, 481–498, doi: 10.1193/082916EQS138M.

Bourne, S. J., S. J. Oates, J. J. Bommer, B. Dost, J. van Elk, and D. Doornhof (2015). A Monte Carlo method for probabilistic seismic hazard assessment of induced seismicity due to conventional gas production, *Bull. Seismol. Soc. Am.* **105,** no. 3, 1721–1738.

Brune, J. N. (1970). Tectonic stress and the spectra of seismic shear waves from earthquakes, *J. Geophys. Res.* **75,** no. 26, 4997–5009.

Brune, J. N. (1971). Correction, *J. Geophys. Res.* **76,** no. 20, 5002.

Campbell, K. W. (2009). Estimates of shear-wave Q and κ_0 for unconsolidated and semiconsolidated sediments in eastern North America, *Bull. Seismol. Soc. Am.* **99,** no. 4, 2365–2392.

Darendeli, M. (2001). Development of a new family of normalized modulus reduction and material damping curves, *Ph.D. Thesis*, Department of Civil Engineering, University of Texas, Austin, Texas.

De Crook, T., and B. Wassing (1996). Opslingering van trillingen bij aardbevingen in Noord-Nederland, *KNMI-RGD Interim Report*, 14 pp. (in Dutch).

De Crook, T., and B. Wassing (2001). Voorspelling van de opslingering van trillingen bij aardbevingen, *Geotechniek* 47–53 (in Dutch).

Elgamal, A., T. Lai, Z. Yang, and L. He (2001). Dynamic soil properties, seismic downhole arrays and applications in practice, in S. Prakash (Editor), *Proc. of the 4th International Conference on Recent Advances in Geotechnical Earthquake Engineering and Soil Dynamics*, San Diego, California, 26–31 March.

Hauksson, E., T. Teng, and T. L. Henyey (1987). Results from a 1500 m deep, three-level downhole seismometer array: Site response, low Q values and $f_{\max}$, *Bull. Seismol. Soc. Am.* **77,** 1883–1904.

Kaklamanos, J., B. A. Bradley, E. M. Thompson, and L. G. Baise (2013). Critical parameters affecting bias and variability in site-response analyses using KiK-net downhole array data, *Bull. Seismol. Soc. Am.* **103,** no. 3, 1733–1749.

Kallioglou, P., T. Tika, G. Koninis, S. Papadopoulos, and K. Pitilakis (2009). Shear modulus and damping ratio of organic soils, *Geotech. Geol. Eng.* **27,** no. 2, 217–235.

Kim, B., Y. M. Hashash, J. P. Stewart, E. M. Rathje, J. A. Harmon, M. I. Musgrove, K. W. Campbell, and W. J. Silva (2016). Relative differences between nonlinear and equivalent-linear 1D site response analyses, *Earthq. Spectra* **32,** no. 3, 1845–1865.

Kishida, T., R. W. Boulanger, N. A. Abrahamson, T. W. Wehling, and M. W. Driller (2009a). Regression models for dynamic properties of highly organic soils, *J. Geotech. Geoenviron. Eng.* **135,** no. 4, 533–543.

Kishida, T., R. W. Boulanger, N. A. Abrahamson, T. W. Wehling, and M. W. Driller (2009b). Regression models for dynamic properties of highly organic soils, *J. Geotech. Geoenviron. Eng.* **135,** no. 4, 533–543.

Kottke, A. (2010). A comparison of seismic site response methods, *Ph.D. Thesis*, Department of Civil Engineering, University of Texas, Austin, Texas.

Kottke, A. R., and E. M. Rathje (2008). Technical manual for Strata, *PEER Report 2008/10*, Pacific Earthquake Engineering Research (PEER) Center, University of California, Berkeley, California.

Kottke, A. R., and E. M. Rathje (2013). Comparison of time series and random-vibration theory site-response methods, *Bull. Seismol. Soc. Am.* **103,** no. 3, 2111–2127.

Kramer, S. L. (2000). Dynamic response of Mercer Slough peat, *J. Geotech. Geoenviron. Eng.* **126,** no. 6, 504–510.

Kruiver, P. P., E. van Dedem, R. Romijn, G. de Lange, M. Korff, J. Stafleu, J. L. Gunnink, A. Rodriguez-Marek, J. J. Bommer, J. van Elk, and D. Doornhof (2017). An integrated shear-wave velocity model for the Groningen gas field, The Netherlands, *Bull. Earthq. Eng.* doi: 10.1007/s10518-017-0105-y.

Kwok, A. O. L., J. P. Stewart, and Y. M. A. Hashash (2008). Nonlinear ground-response analysis of Turkey Flat shallow stiff-soil site to strong ground motion, *Bull. Seismol. Soc. Am.* **98,** no. 1, 331–343.

Lefebvre, G., and D. LeBoeuf (1987). Rate effects and cyclic loading of sensitive clays, *J. Geotech. Eng.* **113,** no. 5, 476–489.

Li, W., and D. Assimaki (2010). Site and ground motion dependent parametric uncertainty of nonlinear site response analyses in earthquake simulations, *Bull. Seismol. Soc. Am.* **100,** no. 3, 954–968

Lunne, T., P. K. Robertson, and J. J. M. Powell (1997). *Cone Penetration Testing in Geotechnical Practice*, EF Spon/Blackie Academic, Routledge Publishers, London, United Kingdom, 312 pp.

McGuire, R. K., W. J. Silva, and C. J. Costantino (2001). Technical basis for revision of regulatory guidance on design ground motions: Hazard- and risk-consistent ground motion spectra guidelines, *NUREG/CR-6728*, U.S. Nuclear Regulatory Commission, Washington D.C.

Menq, F. Y. (2003). Dynamic properties of sandy and gravelly soils, *Ph.D. Thesis*, Department of Civil Engineering, University of Texas, Austin, Texas.

Rathje, E. M., and M. C. Ozbey (2006). Site-specific validation of random vibration theory-based seismic site response analysis, *J. Geotech. Geoenviron. Eng.* **132,** no. 7, 911–922.

Rathje, E. M., A. R. Kottke, and W. L. Trent (2010). Influence of input motion and site property variabilities on seismic site response analysis, *J. Geotech. Geoenviron. Eng.* **136,** no. 4, 607–619.

Rodriguez-Marek, A., E. M. Rathje, J. J. Bommer, F. Scherbaum, and P. J. Stafford (2014). Application of single-station sigma and site response characterization in a probabilistic seismic hazard analysis for a new nuclear site, *Bull. Seismol. Soc. Am.* **104,** no. 4, 1601–1619

Seed, H. B., and I. M. Idriss (1970). Analysis of ground motions at Union Bay, Seattle, during earthquakes and distant nuclear blasts, *Bull. Seismol. Soc. Am.* **60,** no. 1, 135–136.

Stafleu, J., D. Maljers, J. L. Gunnink, A. Menkovic, and F. S. Busschers (2011). 3D modelling of the shallow subsurface of Zeeland, the Netherlands, *Netherlands J. Geosci.* **90,** no. 4, 293–310.

Stewart, J. P., K. Afshari, and Y. M. A. Hashash (2014). Guidelines for performing hazard-consistent one-dimensional ground response analysis for ground motion prediction, *PEER Report 2014/16*, Pacific Earthquake Engineering Research Center, University of California, Berkeley, California.

Toro, G. R. (1995). Probabilistic models of site velocity profiles for generic and site-specific ground-motion amplification studies, *Tech. Rept. 779574*, Brookhaven National Laboratory, Upton, New York.

Tsai, C. C., and Y. M. A. Hashash (2009). Learning of dynamic soil behavior from downhole arrays, *J. Geotech. Geoenviron. Eng.* **135,** no. 6, 745–757.

Wehling, T. M., R. W. Boulanger, R. Arulnathan, L. F. Harder, and M. W. Driller (2003). Nonlinear dynamic properties of a fibrous organic soil, *J. Geotech. Geoenviron. Eng.* **129,** no. 10, 929–939.

Yee, E., J. P. Stewart, and K. Tokimatsu (2013). Elastic and large-strain nonlinear seismic site response from analysis of vertical array recordings, *J. Geotech. Geoenviron. Eng.* **139,** no. 10, 1789–1801.

Charles E. Via, Jr. Department of Civil and Environmental Engineering
Virginia Tech
Blacksburg, Virginia 24061
adrianrm@vt.edu
(A.R.-M.)

Deltares
P.O. Box 85467
3508 AL Utrecht, The Netherlands
(P.P.K., P.M.)

Civil & Environmental Engineering Department
Imperial College London
London SW7 2AZ, United Kingdom
(J.J.B.)

Royal Netherlands Meteorological Institute (KNMI)
Utrechtseweg 297
3731GA De Bilt, The Netherlands
(B.D.)

Nederlandse Aardolie Maatschappij B.V. (NAM)
Schepersmaat 2
9405 TA Assen, The Netherlands
(J.v.E., D.D.)

Manuscript received 18 April 2016;
Published Online 25 September 2017